X-ray- and neutron-scattering measurements of two length scales in the magnetic critical fluctuations of holmium

T. R. Thurston and G. Helgesen*
Department of Physics, Brookhaven National Laboratory, Upton, New York 11973

J. P. Hill
Department of Physics, Brookhaven National Laboratory, Upton, New York 11973 and Massachusetts Institute of Technology, Cambridge, Massachusetts 02139

Doon Gibbs
Department of Physics, Brookhaven National Laboratory, Upton, New York 11973

B. D. Gaulin
Department of Physics, Brookhaven National Laboratory, Upton, New York, 11973 and McMaster University, Hamilton, Ontario, Canada L8S 4M1

P. J. Simpson†
Department of Physics, Brookhaven National Laboratory, Upton, New York 11973
(Received 19 January 1994)

The short-ranged correlations associated with magnetic ordering in the rare-earth antiferromagnet holmium have been characterized in high-resolution x-ray- and neutron-scattering studies. For temperatures within about 2 K above T_N, the short-ranged magnetic fluctuations exhibit two length scales, instead of the single one expected in an ideal system. Well above T_N, the shorter of the two length scales exhibits power-law behavior consistent with normal critical fluctuations; the line shape in momentum space is well described by a Lorentzian, and the measured critical exponents are $\nu=0.54\pm0.04$ and $\gamma=1.24\pm0.15$. The longer of the two length scales is well described by a squared-Lorentzian line shape, and exhibits a power-law temperature dependence. Both the shorter and the longer length-scale fluctuations are approximately spatially isotropic. We propose that the longer length-scale fluctuations are related to random strain fields which are localized at or near the sample surfae. These results are reminiscent of behavior observed at the cubic-to-tetragonal structural phase transitions of some perovskite materials.

I. INTRODUCTION

During the last two years, the short-range correlations associated with magnetic ordering have been characterized in a variety of rare-earth[1-5] and actinide[6,7] antiferromagnets by high-spatial-resolution x-ray- and neutron-scattering techniques. In a number of cases, the magnetic fluctuations have been found to exhibit two length scales instead of the single one expected for an ideal system. The new, longer length scale is localized at or near the sample surface and appears to be correlated with random strain fields. These results are reminiscent of the two length scales observed in earlier x-ray-scattering studies of the cubic-to-tetragonal structural transformations of the perovskites.[8-15] Together, these results for structural and magnetic phase transformations pose an interesting problem in condensed matter physics: How are critical properties of an ideal system altered in the presence of a small degree of disorder or in the neighborhood of a surface, or both?

In this paper we present the results of comprehensive x-ray- and neutron-scattering studies of the critical magnetic fluctuations of holmium. These experiments were motivated, in part, by the intriguing results obtained in the disordered phase of the random-field Ising antiferromagnet $Mn_{0.75}Zn_{0.25}F_2$, in which x-ray- and neutron-scattering experiments gave qualitatively different phase behavior.[16-19] Our intention was simply to observe x-ray critical magnetic scattering, if possible, and to compare the results with those obtained by neutron diffraction on the same sample. Holmium was chosen for its large and reasonably well-understood x-ray resonant magnetic cross section.[20-22] However, it turns out that the magnetic critical behavior of holmium, and indeed of all the rare earths, is still controversial.[23] It seemed possible, therefore, that the complementary strengths of x-ray scattering in comparison to neutron scattering, noted below, might also provide new insights. A summary of our experiments has been published previously.[1]

The main result of this study is that within about 2 K above T_N the magnetic critical scattering exhibits two components, one broad and the other narrow. Thus, instead of a single divergent length scale as predicted for a second-order phase transition in an ideal system, there are two length scales. The two length scales differ in magnitude by a factor of ~ 10 and are both nearly isotropic in all three spatial directions. Assuming that the transition is second order, the critical exponents of the

broad and narrow components (small and large length scales, respectively) can be extracted. These are summarized in Table I. The exponents for γ and ν of the broad component are comparable to theoretical predictions, and the line shape of the scattering is well described by a Lorentzian. From this, we conclude that the broad component arises from normal critical fluctuations. The exponents for the narrow component are quite unusual and are not predicted by any universality class. Its line shape is reasonably described by a squared Lorentzian. We have also found that the narrow component was preferentially detected in our x-ray-scattering experiments, while both components were visible in our neutron-scattering experiments. This difference in sensitivity arises, in part, from the differences in the three-dimensional resolution functions of the x-ray- and neutron-scattering spectrometers. However, this difference may also be related to the differing sample volumes probed by the two techniques. In the current x-ray-scattering experiments (performed at $\hbar\omega \sim 8$ keV), the x-ray penetration depth is approximately 0.5 μm, while the neutron penetration depth is on the order 0.5 cm. Our experiments on holmium samples with three different surface preparations also show that the character of the narrow component is affected by gross surface morphology.

The discovery of critical fluctuations with two-component line shapes in holmium is reminiscent of the two-component line shapes observed in the structural transitions of many perovskite materials.[8-15] There, the second length scale is thought to be nucleated by random defects, at least for weakly first-order transitions.[24] It is possible that our results are the magnetic analog of this phenomenon. Interestingly, the line shapes of the narrow component observed in both the perovskites and holmium are well described (though not uniquely) by a squared Lorentzian, a form often associated with random-field systems. It is also possible that the second length scale is intrinsic, due only to the interface. This line of reasoning was pursued experimentally by Osterman, Mohanty, and Axe[25] in the perovskite $SrTiO_3$ and has been considered theoretically by Lubensky and Rubin.[26] While our current results cannot resolve whether the second length scale originates from defects or is intrinsic to the surface, recent work of Gehring *et al.*[3] and Hirota *et al.*[4] shows that the narrow component is localized predominantly in the sample skin, and not in the bulk. X-ray- and neutron-scattering studies of UO_2 by Watson *et al.*[7] further suggest that the narrow component is correlated with random strains in the near-surface region and may be associated with polishing. In any case, it is clear that the effects of random strains on phase behavior are not well understood and present considerable experimental challenges. Further, these problems are worth understanding, as two-component lines shapes have now been observed in a variety of structural and magnetic phase transformations.

Before turning to the presentation of our experimental results, we briefly note some strengths and weaknesses of x-ray-scattering techniques when applied to magnetic critical phenomena. First, the spatial resolution of x-ray scattering is typically 10 times greater than neutron scattering, and so examination of critical phenomena at temperatures much closer to T_N is possible. Second, the relatively small magnetic cross section for x rays allows extinction-free measurements of the order parameter without any special precautions. Third, the inherently large energy resolution of x-ray spectrometers (typically $\sim 5-10$ eV) allows a complete integration over the energy range of the critical fluctuations (typically ~ 1 meV), which as we discuss below simplifies the analysis of data. One major disadvantage of the magnetic x-ray-scattering technique compared to the neutron-scattering technique is that the x-ray signal rates can be much smaller and the backgrounds higher. This was the case for the nonresonant magnetic x-ray-scattering experiments performed on MnF_2 (Ref. 27) and $Mn_{0.5}Zn_{0.5}F_2$,[28] where the signal from critical fluctuations was too weak to observe over the experimental background.

In Sec. II we describe the magnetic structure of holmium. Experimental details are presented in Sec. III. The magnetic x-ray- and neutron-scattering cross sections are discussed in Sec. IV. We present our data and compare it to current theory in Sec. V. In Sec. VI we speculate on the origin of the second length scale and conclude.

II. MAGNETIC STRUCTURE OF HOLMIUM

The crystal structure of holmium is hexagonal close packed with lattice constants $a = 3.58$ Å and $c = 5.62$ Å at room temperature. In the solid there are ten $4f$ electrons localized at each atomic site and characterized by a Hund's-rule $^5I_8$ configuration. The ordered magnetic moment at low temperatures is large, $\sim 10\mu_B$ per site. Just below the Néel temperature $T_N \sim 131.2$ K, the magnetic moments order ferromagnetically within the hexagonal planes to form a spiral magnetic structure with a turn angle per plane $\phi \sim 50°$ along the c axis.[29] The magnetic diffraction pattern consists of pairs of satellites offset from each of the chemical Bragg reflections by $\Delta\mathbf{Q} = (0,0,\pm\tau)$, where $\tau = 2\phi/c$. The satellite position τ is temperature dependent; at 100 K, $\tau \sim 0.24$ reciprocal lattice units (r.l.u.) (1 r.l.u. $= 2\pi/c = 1.12$ Å^{-1}), while near $T_N \sim 131.2$ K, $\tau \sim 0.28$ r.l.u.[29-31]

Interestingly, the critical properties of holmium near the magnetic ordering transformation are still unclear. Two different universality classes have been proposed for simple spiral antiferromagnets. In the first theory,[32] a Landau-Ginzburg-Wilson (LGW) Hamiltonian was constructed for the symmetric $O(n)$ model with dimensionality $d = 3$ and number of order parameter components $n = 4$. More recently, Kawamura[33] has proposed a generalized LGW Hamiltonian with a fixed point of "chiral" symmetry and an order parameter with $n = 2$ and $d = 3$. The predictions of these two theories for the critical exponents ν, β, γ, and α of holmium are summarized in Table I. The experimentally determined values of the critical exponents, as they have been measured by neutron scattering[34-36] and by heat capacity studies,[37,38] are also shown in Table I. It is clear that neither theory adequately accounts for all of the measured exponents. Indeed, there are also discrepancies evident among exper-

TABLE I. Holmium critical exponents.

Type	Source	α	β	γ	ν
$O(n)$ theory	Ref. 32	−0.17	0.39	1.39	0.70
Chiral theory	Ref. 33	0.40	0.25	1.10	0.53
Experiment	Ref. 34		0.39±0.04		
Experiment	Ref. 36			1.14±0.10	0.57±0.04
Experiment	Ref. 37	0.27±0.02			
Experiment	Ref. 38	0.10–0.22			
This work	Broad component		0.37±0.1[a]	1.24±0.15	0.54±0.04
This work	Narrow component		0.37±0.1[a]	2–5	1.0±0.3

[a]It is impossible to distinguish whether the exponent β found in our experiments should be associated with the broad or narrow component.

imental values for the heat capacity exponent α. A further complication in this regard is the indication of crossover effects in the heat capacity data of Jaysuria, Campbell, and Stewart.[37] Finally, it is worth noting the suggestion of Tindall, Steinitz, and Plumer[39] on the basis of dilatometry measurements that the magnetic ordering transformation has weak first-order character. Along these lines, Barak and Walker[40] have also proposed that the transformation is driven first order by fluctuations, while Azaria, Delamotte, and Jolicouer[41] have proposed that the critical behavior of the spiral rate earths is controlled by tricritical points in their phase diagrams.

III. EXPERIMENTAL DETAILS

Two different samples of holmium were examined in this work. All of the neutron-scattering and most of the x-ray-scattering experiments were performed on a sample with dimensions $9\times4\times4$ mm^3 (sample No. 1). Both c-axis faces of this sample were examined in x-ray-scattering experiments, and they were both prepared by first mechanical polishing and then electropolishing using standard techniques for rare-earth metals.[42] This procedure produced a surface with a mosaic width of 0.008° half-width at half-maximum (HWHM) as measured by x-ray scattering for one of the faces (face No. 1a), and a surface with a mosaic width of 0.048° (HWHM) for the other (face No. 1b). A second sample with dimensions $6\times6\times6$ mm^3 (sample No. 2) was studied in x-ray-scattering experiments. Its c-axis face (face No. 2a) was prepared by mechanical polishing only and gave a reasonably small mosaic width of 0.014° HWHM. No special precautions were taken to reduce possible impurities on the surfaces of any of the samples, and the samples were exposed to air while in storage.

A number of studies have been performed to characterize the surface and near-surface regions of the samples. Scanning ion fluorescence and scanning electron microscopy measurements were done at Oak Ridge National Laboratory on face No. 1a. These studies showed that no unusual chemical impurities were present, but structural defects, such as pits, were evident at micrometer-length scales in the scanning electron microscopy measurements. The mean-square surface roughness as determined by x-ray-reflectivity measurements was 20 Å or greater. Variable-energy positron-annihilation experiments were performed to probe the depth dependence of the defect density along the surface normal direction. The high sensitivity of positron beams to open-volume defects has been applied for this purpose in a variety of metals, semiconductors, and insulators.[43] These studies indicated a high defect density ($\sim10^{18}$ cm^{-3}) extending for a few hundred angstroms beneath the sample surface, with a lower defect density ($\sim10^{16}$ cm^{-3}) extending to a depth of ~0.5 μm. More detailed information concerning the defect type will require systematic studies of several samples with controlled defect densities. These are planned.

Our x-ray- and neutron-scattering experiments were performed at Brookhaven National Laboratory in the National Synchrotron Light Source on beam lines X22C and X25, and in the High Flux Beam Reactor on spectrometer H7. In all experiments the samples were mounted in closed-cycle helium refrigerators (different for the x-ray and neutron experiments) with temperature stability of 0.01 K over several hours. In the x-ray-scattering experiments, the incident photon energy was tuned to ~8071 eV, which corresponds to the dipole maximum of the resonant magnetic scattering at the $L_{\rm III}$ absorption edge ($2p\rightarrow5d$). The neutron spectrometers were operated in an energy-integrating double-axis mode (no analyzer) with an incident neutron energy of $E_i=14.7$ meV and typical collimation 10′-5′-SAMPLE-10′-open.

All of the data in this paper were analyzed by convolving the spectrometer resolution function with the cross section

$$I(\mathbf{Q})=\int R(\xi)\frac{d\sigma}{d\Omega}(\mathbf{Q}-\xi)d\xi\ , \tag{1}$$

where $I(\mathbf{Q})$ is the intensity at momentum transfer $\mathbf{Q}$, $R(\xi)$ is the experimentally measured resolution function, and $d\sigma/d\Omega$ is the cross section. For the x-ray experiments, the experimentally measured resolution function had the approximate form

$$R(\xi)\sim\left[\frac{1}{w_x^2+\xi_x^2}\right]^2\left[\frac{1}{w_y^2+\xi_y^2}\right]^2\left[1-\left|\frac{\xi_z}{w_z}\right|\right], \tag{2}$$

where the x and y directions are transverse and longitudinal to $\mathbf{Q}$ within the scattering plane defined by $\mathbf{k}_i$ and $\mathbf{k}_f$,

and the z direction is out of the scattering plane. The triangular form for the out-of-plane resolution is an approximation which allows the integral of Eq. (1) in the z direction to be performed analytically for certain cross sections. The widths of the squared-Lorentzian forms for the resolution function in the x and y directions were determined by fitting a magnetic peak at temperatures ~ 1 K below the transition temperature. Equation (2) assumes that the resolution function is aligned with principle axis perpendicular and parallel to Q within the scattering plane. Mesh scans around the magnetic peak position performed at $T=115$ K in the ordered phase confirmed the validity of this approximation. The resolution in the x-ray experiments [obtained at the $(0,0,2-\tau)$ reflection] typically had half-width at half-maxima (HWHM$=0.64w_x$, etc.) of 0.000 29, 0.000 45, and 0.0043 Å^{-1} in the transverse, longitudinal, and out-of-scattering-plane directions, respectively.

For the two-axis neutron-scattering resolution function, a form similar to that given in Eq. (2) was used, except that the squared Lorentzians were replaced by Gaussians. Two magnetic peaks were studied in the neutron-scattering experiments. In experiments performed at the $(0,0,2-\tau)$ reflection, the spatial resolution was the lowest with half-widths in the transverse, longitudinal, and out-of-scattering-plane directions of 0.0029, 0.0046, and 0.042 Å^{-1}, respectively. In measurements performed at the magnetic satellite of the origin $(0,0,\tau)$, the transverse resolution was much higher, with half-widths in the transverse, longitudinal, and out-of-scattering-plane directions of 0.000 30, 0.0041, and 0.033 Å^{-1}, respectively. Note that the transverse neutron resolution is comparable in this case to the x-ray resolution. The transverse neutron resolution becomes this fine only when the scattering angle 2θ is small. It is a fortunate aspect of the magnetic scattering in holmium that a satellite peak of the origin exists at small angles so that a high transverse resolution mode ($2\theta\sim 6.6°$ with 14.7-meV neutrons) is attainable. This allows more direct comparisons between x-ray- and neutron-scattering results.

IV. X-RAY AND NEUTRON CROSS SECTIONS

We briefly discuss the x-ray and neutron magnetic scattering cross sections. For both x-ray and neutron scattering, the application of Fermi's golden rule (to second order) gives the following general expression for the cross section of a neutron (photon) with initial momentum $\mathbf{k}_i$ and energy E_i scattered into a state with final momentum $\mathbf{k}_f$ and energy E_f:[44]

$$\left[\frac{d^2\sigma}{d\Omega\, dE_f}\right]=\left[\frac{2\pi\rho(k_f)}{\hbar\Phi}\right]\left|\langle k_f,E_f|H|k_i,E_i\rangle+\sum_n \frac{\langle k_f,E_f|H|n\rangle\langle n|H|k_i,E_i\rangle}{E_i-E_n}\right|^2\delta(E_i-E_f)\ . \tag{3}$$

Here $\rho(k_f)$ is the density of states for the scattered neutrons (photons), Φ the incident flux, and $|n\rangle$ an intermediate state of the system. For the magnetic neutron-scattering experiments described here, the second-order term in the expression above is negligible. Following well-known arguments,[45] the cross section for magnetic neutron diffraction can be manipulated to give

$$\frac{d\sigma}{d\Omega}\sim\langle J^{\mathrm{BP}}(-\mathbf{Q})J^{\mathrm{BP}}(\mathbf{Q})\rangle\ , \tag{4}$$

where $\mathbf{Q}=\mathbf{k}_i-\mathbf{k}_f$ is the neutron momentum transfer and J^{BP} is the (isotropic) basal plane moment of holmium. It has been assumed that the neutron-diffraction experiments are carried out in an energy-integrating mode. Thus the cross section is proportional to the Fourier transform of the instantaneous two-spin correlation function within the basal planes. Using the fluctuation-dissipation theorem, it is possible to relate the neutron cross section to the static susceptibility, which is then typically approximated by a Lorentzian[46] to give

$$\left[\frac{d\sigma}{d\Omega}\right]\sim k_B T\chi(\mathbf{Q},T)\sim\frac{k_B T\chi(T)}{1+(q_a^2+q_b^2)/\kappa_{ab}^2+q_c^2/\kappa_c^2}\ . \tag{5}$$

Here $\mathbf{q}=(q_a,q_b,q_c)$ is the deviation from either the $(0,0,\tau)$ or $(0,0,2-\tau)$ magnetic peak positions, $\chi(T)$ is the amplitude of the susceptibility, and κ_{ab} and κ_c are inverse correlation lengths within the basal plane and along the c axis. In fact, the Lorentzian form given above must be used cautiously. This is because the Lorentzian approximation is valid only for small q. When integrating the product of the susceptibility and the resolution function over momentum space [Eq. (1)], the result may not be mathematically well behaved. One way to modify Eq. (5) to prevent these problems is to include fourth-order terms in the denominator.[47] In this work we shall use the Lorentzian form of Eq. (5), but be careful in interpreting results, especially when κ_{ab} and κ_c become much smaller than the resolution widths.

In a resonant magnetic x-ray-scattering experiment, the energy of the incident photons is tuned near an absorption edge, so that the second-order terms in Eq. (3) are large. The sensitivity of these terms to the magnetization density has been discussed in detail elsewhere.[20–22,44] In the present experiments, the incident photon energy was set near the dipole maximum of the L_{III} absorption edge of holmium. Briefly, $2p$ core electrons are promoted by the incident photons to unoccupied $5d$ states, which subsequently decay through the emission of an elastically scattered photon. The amplitude of the resonant cross section depends on the matrix elements which couple the ground and excited magnetic states allowed by the exclusion principle. The detailed form of the x-ray magnetic cross section, in particular, its application to magnetic critical phenomena, is still an

area of active research.[48–50] Nevertheless, some results seem clear. First, the polarization dependence of the magnetic cross section in a system with spherical symmetry is well understood.[22] For the geometry used in the present experiments (with ~90% σ polarization of the incident beam), the dipole cross section measures the projection of the basal-plane moments along the scattered photon direction $\mathbf{k}_f$.[22] Second, the relatively broad energy resolution (~5–10 eV) characteristic of our experiments ensures a full energy integration and implies that the cross section measures an instantaneous correlation function. Finally, recent calculations suggest[48–50] that the dominant terms in the resonant dipole cross section are proportional to two-spin correlation functions, similar in that regard to neutron diffraction. For these reasons we have assumed in this paper that the x-ray resonant and neutron-scattering magnetic cross sections may be directly compared through Eq. (5).

V. EXPERIMENTAL RESULTS

A. Two-component line shapes

In this section we present our experimental data. We note that all the data were taken by first cooling the sample from ~10 K above the Néel temperature to ~120 K and then heating in small steps. The main results of our work are illustrated in Figs. 1 and 2, where scans of two magnetic satellites are plotted for several temperatures and three experimental configurations. Figure 1 shows transverse scans, which measure the correlation lengths within the basal planes, while Fig. 2 shows longitudinal scans performed under identical conditions, which measure the correlation length along the c axis. High-resolution x-ray-scattering results are shown in the left-hand column of each figure, low-resolution neutron-scattering results in the middle column, and high-resolution neutron-scattering results in the right-hand column. The top rows show scans taken below T_N and illustrate the resolution limits obtained for the respective experimental configurations. As shown in Fig. 1, the high-resolution transverse half-width obtained by neutron scattering at the $(0,0,\tau)$ position is comparable in extent to the x-ray half-width. This resolution corresponds to a correlation length of ~3300 Å and was achieved with reasonable neutron-scattering intensities only when the scattering angle of the spectrometer was small; at the $(0,0,\tau)$ position, $2\theta \sim 6°$. At the $(0,0,2-\tau)$ position, where the scattering angle is large ($2\theta \sim 42°$),

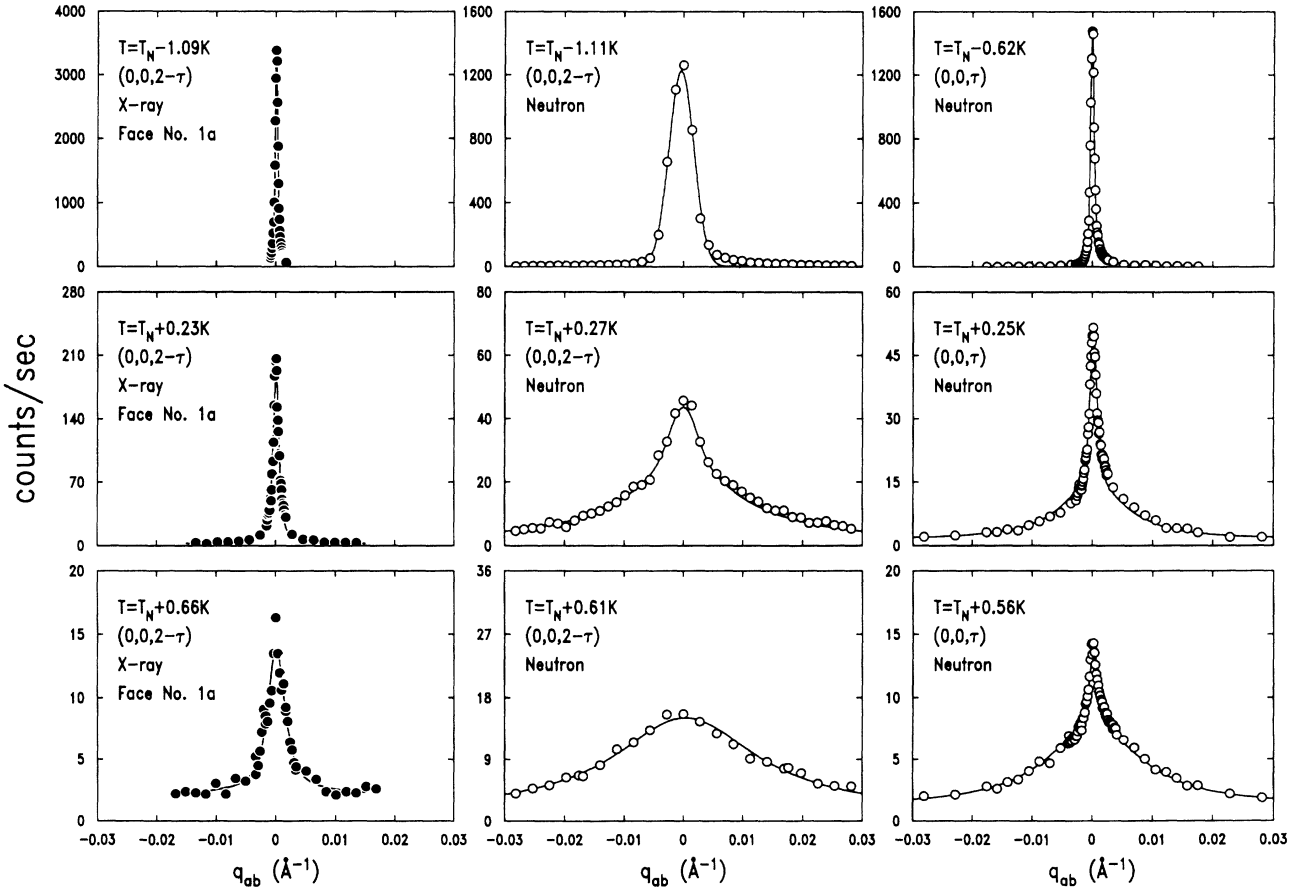

FIG. 1. Transverse x-ray- and neutron-scattering scans taken at the $(0,0,2,-\tau)$ and $(0,0,\tau)$ magnetic peak positions. The scans in the top row of the figure were taken at temperatures below the transition and represent the resolution of the different experimental configurations. The center and bottom rows show critical scattering observed at temperatures above the transition. The solid lines represent fits to the Lorentzian plus squared-Lorentzian line shape discussed in the text.

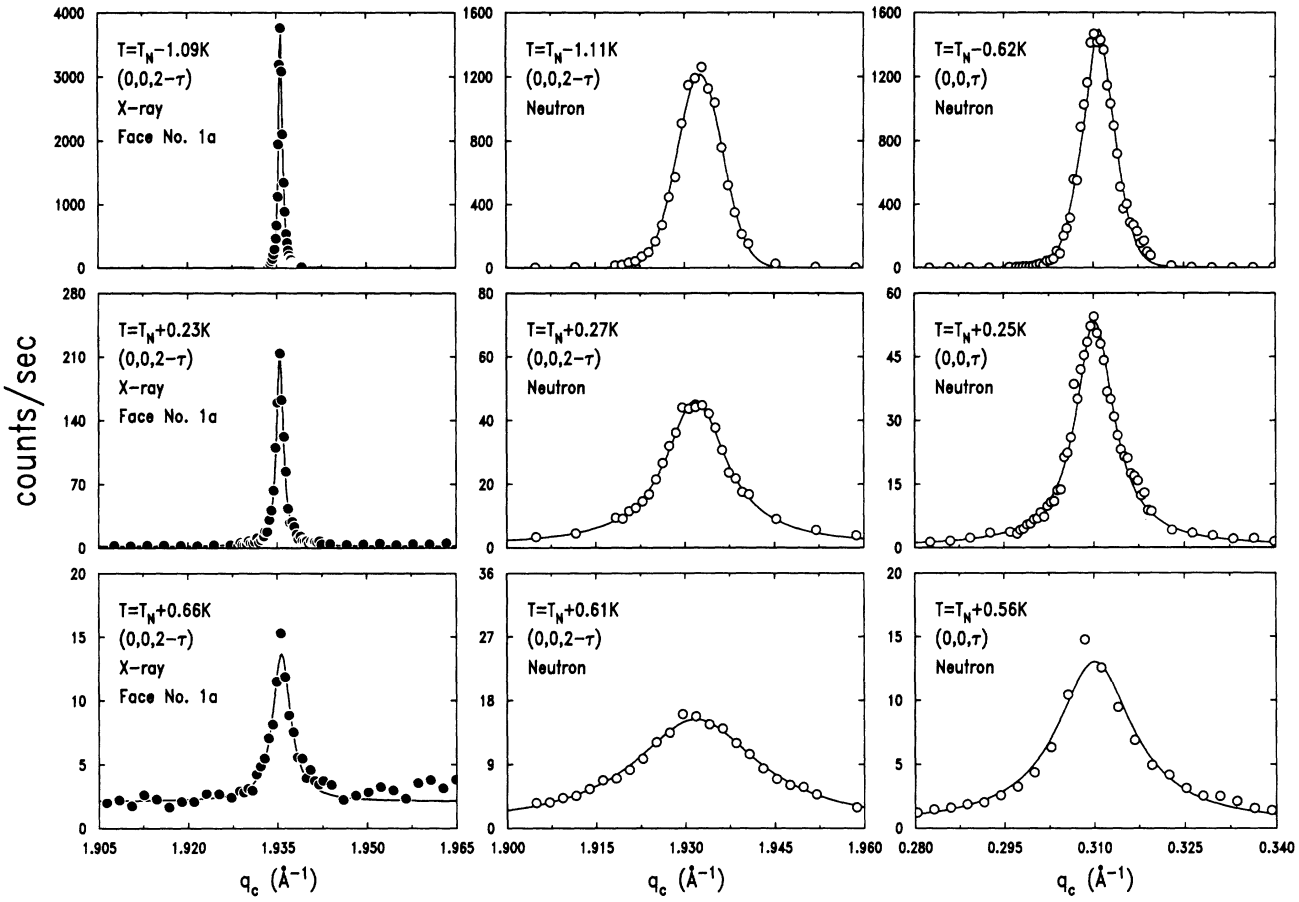

FIG. 2. Longitudinal x-ray- and neutron-scattering scans taken under identical conditions to those of Fig. 1.

Fig. 1 shows that the transverse width obtained by neutron scattering is much larger. The top row of Fig. 2 also shows that the longitudinal neutron resolution at both the $(0,0,2-\tau)$ and $(0,0,\tau)$ positions is much broader than the x-ray resolution. It is noteworthy that the neutron transverse and longitudinal resolution widths at the $(0,0,\tau)$ position are about 9 times more anisotropic than the transverse and longitudinal x-ray resolution widths at the $(0,0,2-\tau)$ position.

The center and bottom rows of Figs. 1 and 2 show scans taken at increasing temperatures above the transition. As may be seen, the amplitudes of the scattering decrease and the widths increase for increasing temperatures, which is qualitatively consistent with the behavior expected for critical fluctuations. The most striking feature of the data is the suggestion of two components in the magnetic scattering. In particular, the data obtained by x-ray scattering [left-hand side (LHS)] preferentially selects the narrower component, while that obtained by low-resolution neutron scattering selects the broader component (middle). Both components are visible in the transverse high-resolution neutron-scattering data shown in Fig. 1 (RHS). Comparison of the longitudinal and transverse x-ray-scattering widths in Figs. 1 and 2 suggests that the correlation lengths of the narrow component within the basal planes and along the c axis have similar magnitudes. The neutron-scattering data also show that the broad component is approximately isotropic. The high-resolution x-ray- and neutron-scattering scans in the left- and right-hand columns of Fig. 1 suggest that the intensity of the narrow component decreases more rapidly with temperature than the broad com-

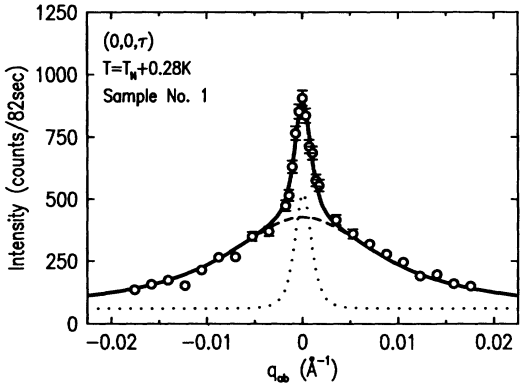

FIG. 3. Transverse neutron-scattering scan taken at the $(0,0,\tau)$ magnetic peak position which emphasizes the two-component nature of the scattering present above the transition. The solid line represents a fit to the Lorentzian plus squared-Lorentzian line shape discussed in the text. The dashed line represents the Lorentzian component of the fit, and the dotted line represents the squared-Lorentzian component.

ponent. In fact, the narrow component was not visible for temperatures ~2 K above T_N in either the x-ray or high-resolution neutron-scattering data, while the broad component was still visible 10 K above the transition.

A high-resolution transverse scan which emphasizes the two-component behavior is shown in Fig. 3. The dashed line represents a Lorentzian description of the "broad component," while the dotted line gives the remaining "narrow component." The choice of a Lorentzian was motivated from earlier studies of magnetic critical fluctuations[23] and is discussed in Sec. V B. From the data in Fig. 3, we are led to the idea that the broad and narrow components arise from separate domains of the sample. Although we have not found a simple, single-component line shape (more sharply peaked than a Lorentzian) which gives a good description of all the data, we cannot rule out this possibility. Our approach has been to denote the extra scattering which cannot be described by a single Lorentzian as the second component. We shall return to a more detailed discussion of the scattering line shapes shortly.

B. Order parameter, incommensurability, and correlation length

The incommensurability τ measured using both x-ray- and neutron-scattering techniques is plotted versus temperature in Fig. 4(a) between 30 and 130 K. The results of the two techniques agree to within instrumental accuracy over the entire temperature range studied. The integrated intensities of magnetic peaks measured using both x-ray and neutron scattering are plotted versus temperature in Fig. 4(b). These data were obtained by fitting transverse scans through the $(0,0,2-\tau)$ magnetic peak and then integrating the fitted curves. For the x-ray-scattering data, the integrated intensity has been scaled and the transition temperature shifted by 0.2 K, so that the neutron and x-ray data overlap near T_N. Since different cryostats were used in the x-ray- and neutron-scattering experiments, these differences in T_N are probably due to errors in measurement of the absolute value of the temperature. For a range of temperatures about 2 K below the transition, the x-ray and neutron data coincide, but for lower temperatures the intensity of the neutron data is smaller than the intensity of the x-ray data. It seems likely that this discrepancy arises from extinction in the neutron-scattering experiments.

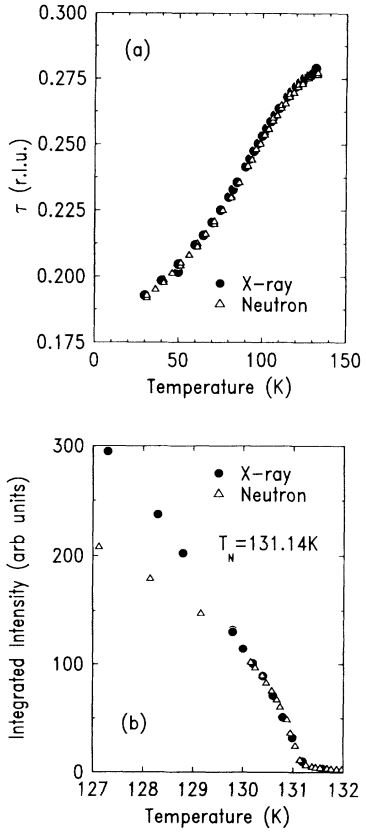

FIG. 4. (a) Magnetic wave vector τ as a function of temperature measured using x-ray and neutron scattering. (b) Integrated intensity of the $(0,0,2-\tau)$ magnetic peak measured using x-ray and neutron scattering.

For each integrated intensity data set taken, the temperature dependence of the magnetic peak intensity within ~1 K below T_N was fitted to a power law $I\sim(T_N-T)^{2\beta}$ in order to determine T_N. These fits revealed variations in T_N from cycle to cycle which were typically about one-tenth of a degree kelvin. Since the same cryostat was used in each of these cycles, it is not known whether the deviations reflect the accuracy of the thermometry, the uncertainty in the determination of β, or possible hysteresis near T_N. The average values for β extracted from fits of the data within ~1 K below T_N were $\beta=0.3\pm0.1$ for neutrons and $\beta=0.37\pm0.1$ for x rays. Again, the apparent differences between our x-ray and neutron results for β probably arise from extinction effects in the neutron-scattering experiments.[51]

An interesting and serious complication in the determination of T_N in these experiments involves the differences obtained by fitting the temperature dependence of the intensities of the magnetic scattering below T_N and of the half-widths of the critical scattering above T_N. This aspect of the data is illustrated in Fig. 5, where the integrated intensity and transverse half-widths of x-ray and low-resolution neutron-scattering data are plotted versus temperature. We note that the half-widths in Fig. 5 result from fits to transverse scans that have *not* been convolved with the experimental resolution function. The important feature of the data shown in Fig. 5 is that the values of T_N determined by power-law fits to the integrated intensity $I\sim(T_N-T)^{2\beta}$ and from power-law fits to the half-width HWHM $\sim(T-T_N)^{\nu}$ differ by about 0.2 K. This is true for both the x-ray- and neutron-scattering data. In earlier analyses of critical scattering, these kinds of differences in the values obtained for T_N have sometimes been attributed to the presence of critical fluctuations below T_N, which broaden the peak while there is still long-ranged order. The ambiguity in determining T_N is then removed by fitting the data to a two-component cross section containing terms for both long-range order and critical fluctuations. The problem in this case is that the narrow component *cannot* be easily dis-

tinguished from the component for long-range order. We are then forced to increase the size of the error bars on power-law fits for all of the critical properties found, such as the values quoted above for the exponent β. The presence of a second length scale in the critical fluctuations near T_N may account for some of the discrepancies reported in earlier determinations of the critical exponents and in the comparison of these with theory.

One way to analyze the line shapes of the x-ray- and neutron-scattering data is suggested by previous work on structural phase transitions in perovskite materials.[8–15] Two-component line shapes have also been observed in these systems, and the longer length scale fluctuations are thought to nucleate at randomly distributed structural defect or chemical impurity sites. We discuss this interpretation further in Sec. VI. In this scenario the narrow component has a squared-Lorentzian line shape, and so with a Lorentzian for the normal critical fluctuations, the total magnetic cross section is

$$I(\mathbf{q}) \sim \frac{\chi_1}{1+(q_a^2+q_b^2)/\kappa_{ab}^2+q_c^2/\kappa_c^2} + \frac{\chi_2}{[1+(q_a^2+q_b^2)/\sigma_{ab}^2+q_c^2/\sigma_c^2]^2} . \quad (6)$$

Here χ_1 is the susceptibility of the normal and critical fluctuations, χ_2 is the susceptibility of the longer length scale fluctuations, κ_{ab} and σ_{ab} are inverse correlation lengths within the basal plane, and κ_c and σ_c are inverse correlation lengths along the c axis. The solid lines through the data in Figs. 1 and 2 represent fits to Eq. (6) convolved with the experimental resolution function. For the x-ray data, the width of the Lorentzian term was determined by the neutron-scattering results obtained at the same reduced temperature.

The Lorentzian plus squared-Lorentzian line shape provided a satisfactory description of the data, as shown in Figs. 1–3. However, this description is not unique. In deciding how to fit the data, we have been guided mostly by the high-resolution neutron-scattering results. At high temperatures these data are well fit by a single Lorentzian term, and so we included this term to describe the broad component. For the narrow component, fits of the high-resolution neutron-scattering data to Eq. (6) above gave an average goodness-of-fit parameter $(\chi^2) \sim 15\%$ lower than fits to a line shape where both the broad and narrow components were fitted to simple Lorentzians. On the other hand, the narrow component observed in the x-ray-scattering experiments had an average value of χ^2 which was $\sim 15\%$ higher when the line shape given in Eq. (6) was used than when a single-component Lorentzian was used. When considering the combined x-ray and neutron data sets, the two-component line shape given above seemed most suitable. A feeling for how the widths depend on the line shape chosen for the fitting can be gained from Fig. 6. Here transverse x-ray-scattering scans have been fitted to a nonconvolved Lorentzian, a convolved Lorentzian, and the sum of a Lorentzian plus squared Lorentzian (with the Lorentzian width set equal to the neutron-scattering value determined for the broad component). The half-widths of the narrow component extracted from these three types of fits all have the same linear temperature dependence. In this regard the data analysis is not particularly sensitive to the line shape chosen. However, the magnitudes of the half-widths differ when the data is fitted to different line shapes.

The half-widths κ_{ab} of the broad component are shown over a large temperature range in Fig. 7. The inset shows

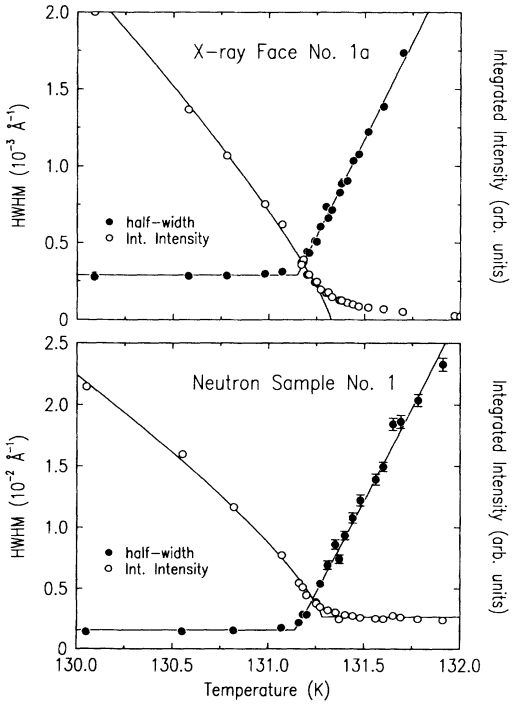

FIG. 5. Integrated intensity and half-width (HWHM) of transverse scans taken at the $(0,0,2-\tau)$ peak position. These data were extracted from fits with no deconvolution performed. The solid lines represent power-law fits discussed in the text.

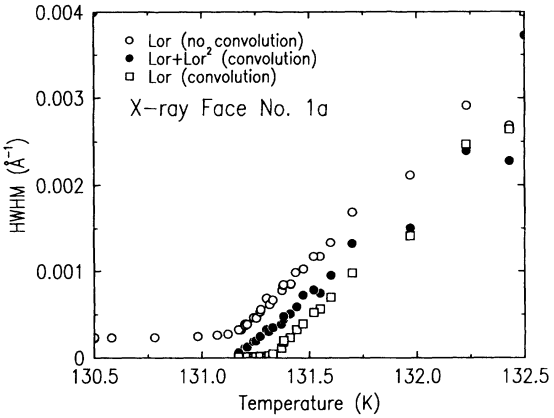

FIG. 6. Temperature dependence of the half-width of transverse x-ray-scattering data found using three different methods of fitting. The open circles represent half-widths extracted from fits to a nonconvolved Lorentzian, the open squares from a Lorentzian convolved with the resolution function, and the solid circles from a Lorentzian plus squared Lorentzian convolved with the resolution function.

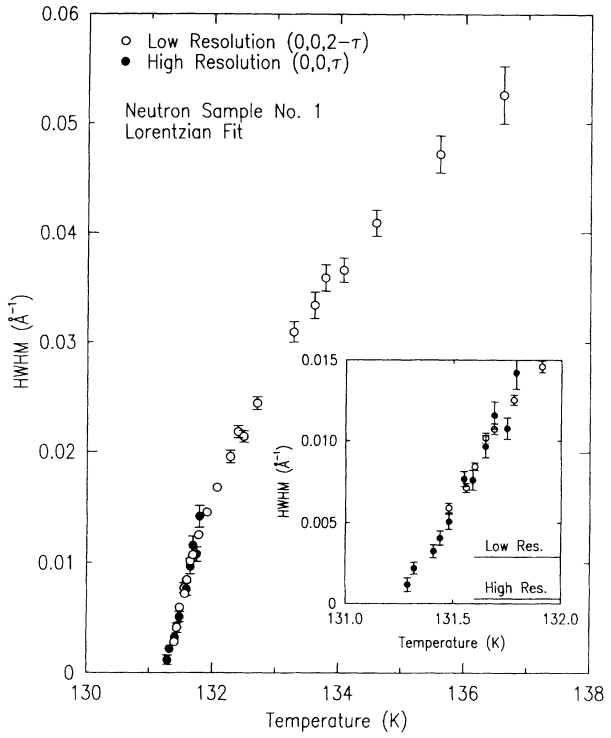

FIG. 7. Transverse half-widths of the broad component found from neutron-scattering data. The solid circles are from high-resolution data taken at the $(0,0,\tau)$ magnetic peak position, and the open circles are from low-resolution data taken at the $(0,0,2-\tau)$ position. The fits used to extract this data are described in the text. The inset shows the temperature dependence close to the transition. The resolution limits for the two configurations are shown to the right of the data in the inset. The low-resolution limit is identified by "Low Res.," while the high-resolution limits is identified by "High Res."

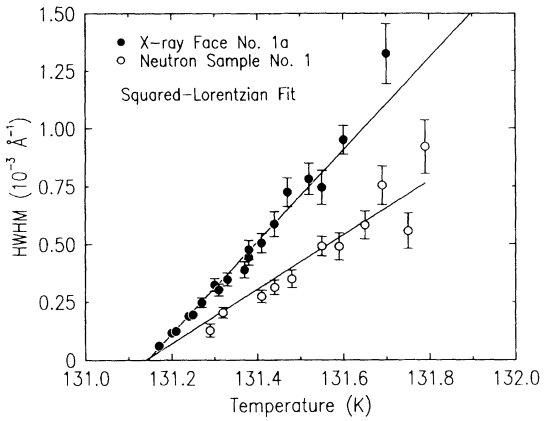

FIG. 8. Transverse half-widths of the narrow component found from fits to a squared Lorentzian. The solid circles represent x-ray-scattering data, and the open circles represent high-resolution neutron-scattering data.

the temperature dependence close to the transition. The solid circles represent the results of Eq. (6) convolved with the experimental resolution function and fitted to the high-resolution neutron data. For the low-resolution neutron-scattering data, a single Lorentzian was convolved with the resolution function, and the results of these fits are represented by open circles in Fig. 7. Additional points in the low-resolution data set for temperatures below 131.5 K were removed because their widths suggested that the narrow component dominated the scattering. In fact, the narrow component persists up to ~132 K, but between 131.5 and 132 K, the broad component dominates the scattering. This is confirmed by data for the half-width obtained at high and low resolution which overlap in this temperature range. The broad component exhibits power-law behavior for temperatures ~2 K above the transition, but within ~2 K of T_N, the power-law behavior breaks down.

Figure 8 shows the temperature dependence of the transverse half-widths of the narrow component $(0.64\sigma_{ab})$ extracted from fits to Eq. (6) convolved with the experimental resolution function. Open and solid symbols give the results of neutron- and x-ray-scattering experiments, respectively. The magnitudes of the half-widths of the transverse component for both x-ray and neutron scattering are comparable, although they differ by up to a factor of ~2 at some temperatures. It is not currently known why the x-ray and neutron half-widths do not agree quantitatively. It is possible that the distribution of narrow and broad components varies with distance from the surface of a sample, with the broad component more pronounced in the bulk and the narrow component prevalent within several micrometers of the surface. Then, depending on the x-ray penetration depth, the wings of the measured line shape might be enhanced (or reduced), thereby changing the apparent width. Along these lines, x-ray-scattering data to be presented in detail below show that the width of the narrow component appears to be correlated with surface preparation.

Figure 9 shows transverse half-widths of the critical scattering plotted against the reduced temperature $t=(T-T_N)/T_N$ on a log-log scale. These data were all extracted from fits to Lorentzian plus squared-Lorentzian line shapes convolved with the experimental resolution functions. Open and solid symbols give the results of neutron- and x-ray-scattering experiments, respectively. The temperature at which the narrow component diverged (131.14 K) was used for T_N in calculating the reduced temperature t. The results illustrated in Fig. 9 show that the broad and narrow components differ by a factor of ~10 in magnitude at comparable reduced temperatures. While the temperature dependence of the width of the narrow component as detected by x rays shows power-law behavior when $T_N=131.14$ K, the neutron-scattering data for the broad component do not follow a single power law over the entire temperature range for which it was observed. This conclusion holds even when the transition temperature used in calculating the reduced temperature $t=(T-T_N)/T_N$ is varied. The breakdown in power-law behavior of the broad component occurs in the temperature range when the narrow component first becomes observable, which suggests that

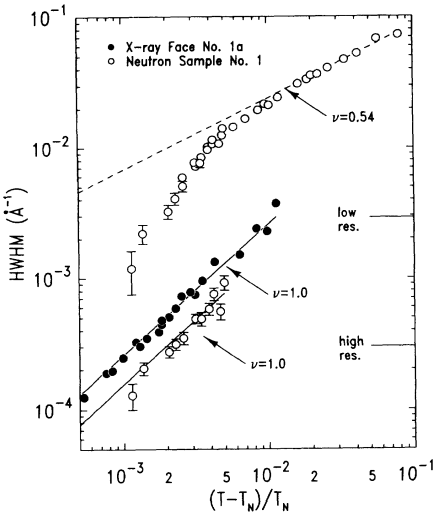

FIG. 9. Half-width at half-maxima (HWHM) of the broad and narrow components for transverse scans. T_N in the reduced temperature $(T-T_N)/T_N$ has been fixed at the temperature where the narrow component diverges, 131.14 K. The solid lines through the data represent fits to a power law $\mathrm{HWHM}=\kappa_0[(T-T_N)/T_N]^{\nu}$. The resolution limits for the various configurations are shown to the right of the data. The low-resolution neutron-scattering limit is identified by "low res.," while the x-ray and high-resolution neutron-scattering limits are identified by "high res."

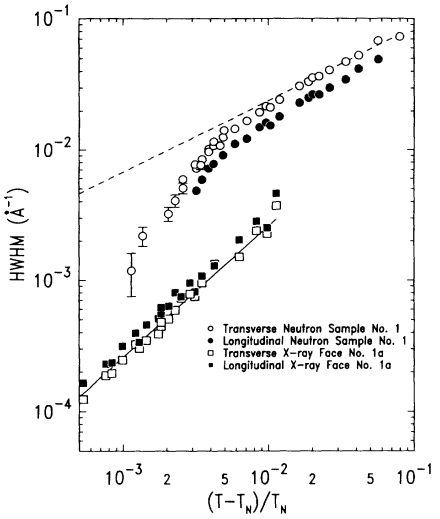

FIG. 10. Transverse and longitudinal half-widths extracted from fits to a Lorentzian plus squared Lorentzian convolved with the experimental resolution function. The transverse data are the same as those plotted in Fig. 9, and the longitudinal data come from similar fits. T_N in the reduced temperature $(T-T_N)/T_N$ has been fixed at the temperature where the narrow component diverges, 131.14 K.

the two phenomena are related. Fitting the data in Fig. 9 to a power-law form for the half-widths, $\mathrm{HWHM}=\kappa_0 t^{\nu}$, we have extracted the value $\nu=1.0\pm0.2$ for the exponent of the narrow component of the x-ray-scattering data. For the neutron-scattering data, we find $\nu=1.0\pm0.3$ for this component. For the broad component detected by neutron scattering, fits to the data for temperatures larger than ~ 2.5 K above the transition gave $\nu=0.54\pm0.04$. The large error bars for the values of the exponents quoted above arise almost entirely from the uncertainty in determining T_N.

Figure 10 shows both longitudinal and transverse half-widths plotted versus the reduced temperature. X-ray-scattering data in the transverse and longitudinal directions are represented by open and solid squares respectively, while neutron-scattering data in the transverse and longitudinal directions are represented by open and solid circles. The transverse data are the same as that presented in Fig. 9, and the longitudinal data were extracted using identical fitting procedures. No high-resolution neutron-scattering data are shown for the narrow component in the longitudinal direction, since only its transverse width could be cleanly resolved with this technique. The longitudinal widths measure correlation lengths along the c axis, while the transverse widths measure basal-plane correlations. The half-widths measured along the c axis had exponents ν similar to those within the basal planes, but their amplitudes were slightly larger along the c axis for the narrow component detected by x-rays and smaller for the broad component detected by neutrons. Nonetheless, it follows from Fig. 10 that the broad and narrow components are approximately *isotropic* over the entire temperature range studied.

The temperature dependence of the amplitudes for the broad and narrow components [χ_1 and χ_2 in Eq. (6)] are shown in Fig. 11. These results are plotted on a log-log scale versus the reduced temperature $t=(T-T_N)/T_N$ with $T_N=131.14$ K (the temperature where the width of the narrow component diverged). The open and solid circles represent the results of neutron- and x-ray-scattering experiments, respectively. All of the data were extracted

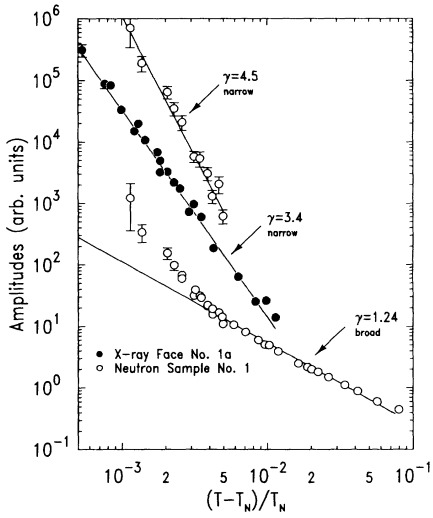

FIG. 11. Fitted amplitudes χ_1 and χ_2 of the broad and narrow components. T_N in the reduced temperature $(T-T_N)/T_N$ has been fixed at the temperature where the narrow component diverges, 131.14 K. The solid lines through the data represent fits to a power law $\chi_1\sim[(T-T_N)/T_N]^{-\gamma}$. X-ray-scattering data are represented by solid circles and neutron-scattering data by open circles.

from fits to Eq. (6) convolved with the experimental resolution function. Note that the x-ray- and neutron-scattering data are not shown on an absolute scale, so that their relative magnitudes cannot be compared. The value of the exponent γ for χ_2 of the sharp component varies from 2 to 5, depending on the value of T_N used in calculating the reduced temperature. This exponent cannot reasonably be said to have been established in these experiments. However, we can conclude that it is not in agreement with any theoretical predictions[32,33] (see Table I). For the broad component, χ_1 exhibits power-law behavior only when $T-T_N$ is greater than ~ 1 K. Over this temperature range, the fitted value for the exponent γ was $\gamma = 1.24 \pm 0.15$. This value agrees within the errors with both the $O(n)$ and chiral model renormalization-group calculations.

C. Comparison to theory

The values of the exponents determined in these experiments are collected in Table I, separately for the broad and narrow components. In fitting the data to extract these exponents, we have assumed that the magnetic ordering transformation is continuous, so that this procedure is sensible. It should be recalled, however, that this assumption may be incorrect and indeed is made less clear by the presence of a second sharp component near T_N. Bearing these complications in mind, several points are immediately clear. The measured exponents for the sharp component are very different from those measured for the broad component or by any earlier neutron-scattering experiments. Furthermore, they do not correspond to the values of any known universality class. In contrast, the measured exponents for the broad component agree to within the errors with those determined by earlier neutron-scattering experiments. This supports our suggestion that it is the broad component corresponding to the classical critical fluctuations which has been characterized most often. Despite this agreement among experiments, neither theory satisfactorily accounts for all of the exponents. The chiral universality class[33] fails to predict β, while the $O(4)$ model[32] fails to predict ν.

D. Differences in x-ray- and neutron-scattering line shapes

Comparison of the scans in the middle and bottom rows of Figs. 1 and 2 indicates that the narrow component is preferentially detected by x-ray scattering, while the broad component is dominant in the low-resolution neutron-scattering data. As noted above, the low-resolution neutron-scattering results agree with previous magnetic neutron-scattering experiments[36] which were all performed in a low-resolution configuration, and this explains why the narrow component has remained undetected until now. It is important to understand why the narrow component is so clearly visible in the x-ray-scattering experiments. One aspect of the explanation for this difference arises from the relatively small size of the x-ray resolution function compared to the neutron resolution function. Figure 12(a) depicts the convolution of the x-ray and neutron resolution functions with a model two-component line shape in a transverse scan. The ellipses in the left part of the figure show the resolution functions of the two instruments. As noted above, the neutron resolution half-width in the longitudinal (and out-of-scattering plane) direction is large compared to the x-ray resolution width, but the widths in the transverse direction are comparable. The neutron resolution ellip-

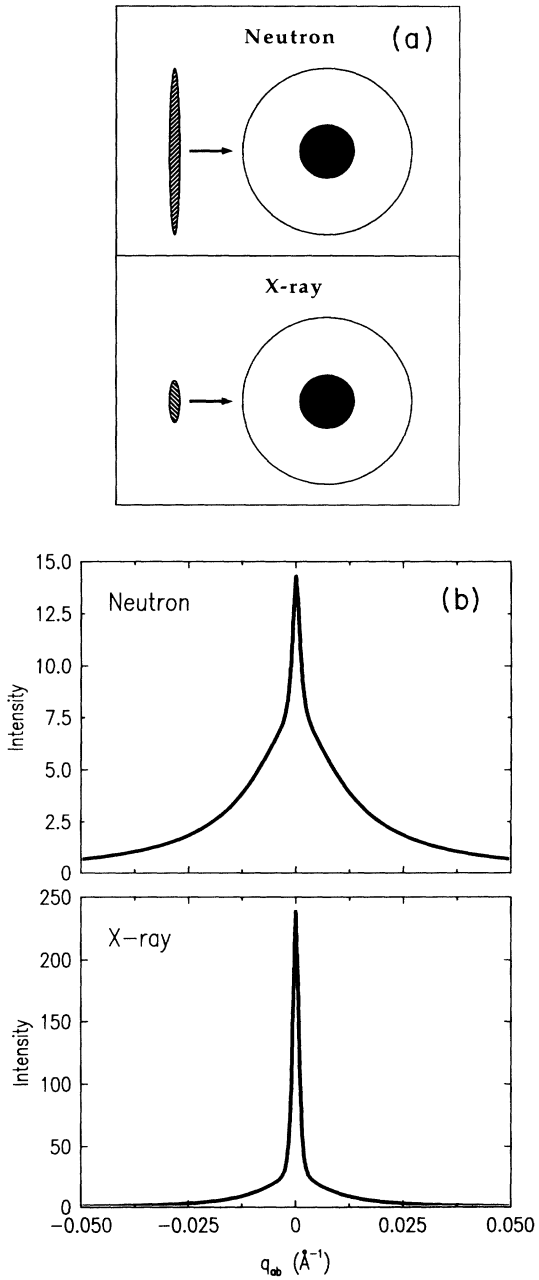

FIG. 12. (a) Pictorial representation of the x-ray and neutron resolution functions being scanned transversely through a two-component line shape. (b) Simulations of transverse scans where identical Lorentzian plus squared-Lorentzian line shapes have been convolved with the x-ray- and neutron-scattering resolution functions. The difference in visibility of the broad component here arises solely from resolution effects.

soid is consequently much more anisotropic than the x-ray resolution ellipsoid. The circles to the right of the figures represent the scattering from a two-component function, with the solid-circle representing the narrow component and the outer circle the broad component. When a scan is performed, the scattering is integrated over the resolution function at each point. From the figure it is easy to see how the broad component is more easily detected by the neutron resolution function once this integration is taken into account. This is confirmed in Fig. 12(b), where identical two-component Lorentzian plus squared-Lorentzian line shapes were convolved with both the x-ray and neutron resolution functions. For the neutron simulation, both components are clearly visible, while in the x-ray simulation the broad component is so weak that it is difficult to distinguish the broad component from the tails of the narrow component or the scattering background. Thus it is possible to explain the differences observed in the x-ray- and neutron-scattering line shapes solely on the basis of the differences in the resolution functions.

Another possible explanation is that the narrow component of the scattering originates in a volume of the sample near the surface, that is, in the "skin." Because the x-ray penetration depth in holmium at 8.071 keV is only ~ 0.5 μm, it is plausible that x-ray scattering is mainly sensitive to near-surface properties, in contrast to neutron scattering, which probes the bulk. To gain more information in this regard, we performed x-ray-scattering experiments on two additional samples with mosaics of 0.014° HWHM (face No. 2a) and 0.048° HWHM (face No. 1b). We note that both of these faces were mechanically polished. However, only face No. 1b was subsequently electropolished, in order to reduce the damage left from mechanical polishing. In fact, face No. 1b was prepared in a manner identical to that of the primary sample, face No. 1a. Figure 13 shows the half-widths of transverse scans taken on all three samples as a function of temperature. These data were extracted from fits where *no* deconvolution was performed. The half-widths at temperatures below the transition represent the mosaic, which is one measure of the degree of disorder present in the region of the sample probed by x-ray scattering. Above T_N, the measured half-widths for all samples exhibited power-law behavior $\kappa_0 t^{\nu}$ with $\nu \sim 1$. From the measured values of ν, we infer that the narrow component is preferentially detected in all three samples. The lines in Fig. 13 represent power-law fits with $\nu = 1$. After subtracting the mosaic width, values for κ_0 extracted from the data of Fig. 13 with $\nu = 1$ were 0.32 Å^{-1} (face No. 1a), 0.58 Å^{-1} (face No. 1b), and 0.82 Å^{-1}, (face No. 2a). Although these experiments show that the behavior of the narrow component observed with x rays is affected by the gross surface morphology (presumably through strain fields), they do not prove that the narrow component originates at the surface.

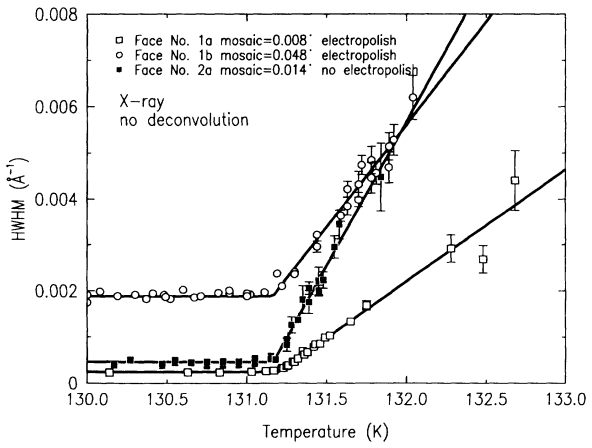

FIG. 13. Transverse x-ray-scattering half-widths of samples with three different surface preparations. The width below the transition is proportional to the mosaic. The lines represent power-law fits HWHM $=\kappa_0[(T-T_N)/T_N]^{\nu}$ with $\nu = 1$.

VI. DISCUSSION

A central issue in the present work is to understand the physical origin of the second, longer length scale observed in these experiments. In our earlier paper,[1] we considered two related mechanisms. In the first, the longer length scale is thought to arise from a random strain distribution, associated with the presence of structural defects. In the second, it is correlated directly with the surface.

Defect-related mechanisms for a second length scale in the critical fluctuations were originally proposed for cubic-to-tetragonal structural transitions in the perovskites. In these systems, inelastic neutron-scattering experiments on strontium titanate also revealed the presence of short-ranged structural correlations with two time scales, with the longer time scale associated with a "central peak" in an energy transfer scan.[52–54] X-ray-scattering experiments subsequently revealed the presence of structural correlations with two length scales.[8–15] Recent neutron-scattering experiments have been interpreted as indicating that the second length scale is not directly related to the second time scale in $SrTiO_3$.[55] For the two length scales, the diffraction line shape in momentum space was fitted to two components, a broad one originating from a soft phonon mode and a second narrow component. While the origin of the narrow component is not understood in detail, it is generally believed that random defects or impurities nucleate domains with a longer length scale. This has been inferred primarily from experiments by Ryan *et al.*[9] in which samples were intentionally doped with impurities. It was found that samples with higher defect or impurity concentrations had more intense scattering in the narrow component. In this context the authors of the work on the two-length-scale problem in the perovskites have suggested that the theory of Imry and Wortis[24] is a useful starting point for interpreting the experiments. We shall return to this argument later.

We now consider the role that the surface may play in giving rise to the narrow component. No definitive conclusions can be drawn on this subject from the data

presented above. However, a set of experiments[3,4] performed at NIST on terbium, a material with magnetic properties very similar to those of holmium, suggested that the narrow component scattering originates predominately in a skin region of the sample. In this work, a 300-μm-wide neutron beam was used to profile the relative intensities of the broad and narrow components as the sample was translated through the beam. Although present at all times, it was found that the intensity of the narrow component was 2 times stronger near the surface than in the bulk of the sample. The intensity of the broad component was independent of sample translation. Deconvolution of the data indicated that the narrow component was strongest in a region ~ 0.3 mm from the surface. In our view these results suggest that the sharp component is present throughout the sample, but more pronounced within the sample skin. It seems very natural to conclude that the sharp component is associated with strains arising from defects and that the defect concentration increases near the surface (within several micrometers at least) as a result of damage upon polishing. The data in Fig. 13 are consistent with such a scenario. Of course, we cannot rule out the possibility that the second length scale is intrinsic to a surface, independent of the strains associated with polishing, although we find this explanation less plausible. Perhaps the strongest current support for a defect-related model comes from experiments done on UO_2.[7] In this case, the narrow component could not be observed with x rays on a smooth surface. When this same surface was mechanically roughened to introduce defects, a second narrow component became visible. A program to test these ideas in which the near-surface defect density is profiled using positron annihilation has been initiated. The goal of this program is to prepare samples which show high and low near-surface defect densities and then determine whether the strength of the narrow component is correlated with the defect density.

Assuming that the second length scale is most likely associated with random strains, we now consider modifications to the qualitative theory of Imry and Wortis[24] necessary to describe our experimental results. In this model the free energy is assumed to be lowered in some regions surrounding defects or impurities. Thus a domain will form around a defect center, provided that the interface energy is not too large. The total free-energy density of such a domain may be written as

$$E_{\text{total}} = E_{\text{wall}} - E_{\text{defect}} \ . \tag{7}$$

The form of the energy of the interface, E_{wall}, depends on the symmetry of the order parameter. In general, $E_{\text{wall}} \sim \sigma l^{\lambda}$, where σ is the surface tension and l is the size of the domain nucleated by the defect. Normally, $\lambda = d-1$, but there are special situations when the walls of the domains become broad, and then $\lambda = d-2$.[24] The form of the free energy associated with a strained region considered here, E_{strain}, will differ from that calculated by Imry and Wortis for defects, E_{defect}. Here we can directly relate the gain in free energy to strain fields by using the Landau free-energy density

$$F = \tfrac{1}{2}a(T-T_N)\Phi^2 + u\Phi^4 + \tfrac{1}{2}ag\Phi^2 + \cdots \ , \tag{8}$$

where Φ is the order parameter. As first emphasized by Axe [56], the term coupling the order parameter and the strain, $g\Phi^2$, has this form in both the magnetic and structural systems where two length scale phenomena have been observed. The particular strain fields which will couple to the order parameter depend on the system. From equation (8), it is clear that the local strain fields g will cause local variations in the transition temperature,[56] since this term enters in the same order as the first term on the right-hand side of Eq. (8). To calculate the gain in free energy that will occur in the region of a strain field, we note that this difference is the same as the difference in free energy of the nonstrained system evaluated at $(T-T_N)$ and $(T-T_N+g)$. Expanding this difference to first order in g gives the following expression for the local change in free energy:

$$F(T-T_N+g)-F(T-T_N) \approx g\left[\frac{\partial F(T-T_N)}{\partial (T-T_N)}\right] = gF' \ . \tag{9}$$

The total gain in free energy in a domain of size l will be the integral of Eq. (9) over the size of the domain. The case analogous to that considered by Imry and Wortis would have l larger than all strain fields. Then the integral is proportional to $l^{d/2}$. This follows from the central-limit theorem and is equivalent to the statement that in a domain of size l in which there is a free-energy gain, $\sqrt{N} \sim l^{d/2}$ of the spins will contribute. An identical argument has been given for the random-field problem by Imry and Ma.[57] Its seems plausible in the current situation, however, that the random strain fields are much larger than the magnetic domains nucleated within them. Then the gain in free energy will have the form

$$E_{\text{total}} = E_{\text{wall}} - E_{\text{strain}} \sim \sigma l^{\lambda} - F' \int_0^l g(\mathbf{r}) d^3\mathbf{r} \ , \tag{10}$$

where $g(\mathbf{r})$ is the functional form of a strain field centered at the origin. The strain field function $g(\mathbf{r})$ in Eq. (10) could represent an average of a distribution of strain fields, or it may be that only a particular type of strain field efficiently nucleates longer length scale domains.

The optimal value for the domain size l is found by minimizing Eq. (10). At this point we mention that the total energy of the domain within the strain field is minimized, rather than the energy density, as was done by Imry and Wortis.[24] This is because our model has only one domain within any strain field, while in the Imry-Wortis scenario, a single domain *or* multiple domains may form in any given volume. For spherically isotropic domains (as assumption which is plausible for holmium, since the narrow component is isotropic), minimizing Eq. (10) with respect to the domain size l yields the relation

$$\frac{l^{\lambda-3}}{g(l)} = \frac{4\pi F'}{\sigma\lambda} \ . \tag{11}$$

For a second-order transition, the surface tension scales as $\sigma \sim t^{2-\alpha-\nu}$ (Ref. 24) and the free-energy density as $F \sim t^{2-\alpha}$. Thus $F' \sim t^{1-\alpha}$.[24] Assuming a power-law de-

cay for the strain field $g(l) \sim l^{-a}$ with $a \approx 1.5$ and $\lambda = d - 1 = 2$,[58] Eq. (11) produces the following temperature dependence for the domain size l:

$$l \sim t^{-2(1-\nu)} \sim t^{-2(1-0.54)} \sim t^{-0.92} . \quad (12)$$

This agrees to within the errors with our experimental temperature dependence for the narrow component. The model makes sense, however, only if the strain fields actually have a $g(l) \sim l^{-1.5}$ dependence over length scales on the order of 200–5000 Å. For elastic deformations, this seems unlikely. However, the strain fields associated with plastic deformations involving multiple defect centers are unknown and might have this dependence. A specific test would be to create specific defect centers in a defect-free sample, such as through ion implantation, where the strain fields could be calculated from first principles. Hopefully, our discussion in this section will motivate further experiments and calculations.

In conclusion, we have demonstrated that the magnetic critical fluctuations in the spiral antiferromagnet holmium exhibit two length scales. The smaller of the two length scales appears to originate from conventional critical fluctuations, while the origin of the longer length scale is not currently understood. The most likely mechanism for producing the second length scale appears to involve strain fields localized at or near the surface. Already, evidence for similar phenomena has been found in other magnetic systems such as NpAs,[6] terbium,[3,4] and UO_2.[7] In our view it seems possible that these effects could be more common in magnetic systems than has previously been realized, and they may explain discrepancies between theoretical and experimental values for critical exponents in other materials.[59]

ACKNOWLEDGMENTS

Helpful conversations with J. D. Axe, R. A. Cowley, C. F. Majkrzak, M. Pacszuski, L. Berman, M. Blume, P. M. Gehring, G. H. Lander, S. Langridge, J. E. Lorenzo, K. Lynn, S. G. J. Mochrie, S. M. Shapiro, G. Shirane, W. G. Stirling, and D. M. Zehner are gratefully acknowledged. The Solid State Division of ORNL and the MIT MRL are acknowledged for their assistance in performing the scanning electron microscopy and scanning ion fluorescence measurements. Work performed at Brookhaven is supported by the U.S. DOE under Contract No. DE-AC02-76-CH00016. J.P.H. received support from NSF Grant No. DMR 90-07825. B.D.G. acknowledges financial support from NSERC of Canada, OCMR of Ontario, and the Alfred P. Sloan foundation. G.H. acknowledges the Research Council of Norway of financial support.

*Permanent address: Institutt for Energiteknikk, N-2007 Kjeller, Norway.

†Permanent address: University of Western Ontario, London, Ontario, Canada N6A 3K7.

[1]T. R. Thurston, G. Helgesen, Doon Gibbs, J. P. Hill, B. D. Gaulin, and G. Shirane, Phys. Rev. Lett. **70**, 3151 (1993).

[2]T. R. Thurston, G. Helgesen, Doon Gibbs, J. P. Hill, B. D. Gaulin, and G. Shirane, Physica B **192**, 177 (1993).

[3]P. M. Gehring, K. Hirota, C. F. Majkrzak, and G. Shirane, Phys. Rev. Lett. **71**, 1087 (1993).

[4]K. Hirota, G. Shirane, P. M. Gehring, and C. F. Majkrzak, Phys. Rev. B **49**, 11 967 (1994).

[5]G. Helgesen, J. P. Hill, T. R. Thurston, Doon Gibbs, R. J. Kwo, and M. Hong (unpublished).

[6]S. M. Langridge, W. G. Stirling, G. H. Lauder, J. Rebizant, J. C. Spirlet, D. Gibbs, and O. Vogt, Europhys. Lett. (to be published).

[7]G. M. Watson, B. D. Gaulin, T. R. Thurston, Doon Gibbs, P. J. Simpson, and G. H. Lander (unpublished).

[8]S. R. Andrews, J. Phys. C **19**, 3721 (1986).

[9]T. W. Ryan, R. J. Nelmes, R. A. Cowley, and A. Gibaud, Phys. Rev. Lett. **56**, 2704 (1986).

[10]U. J. Nicholls and R. A. Cowley, J. Phys. C **20**, 3417 (1987).

[11]A. Gibaud, T. W. Ryan, and R. J. Nelmes, J. Phys. C **20**, 3833 (1987).

[12]A. Gibaud, R. A. Cowley, and P. W. Mitchell, J. Phys. C **20**, 3849 (1987).

[13]S. R. Andrews, Phase Transit. **11**, 181 (1988).

[14]D. F. McMorrow, N. Hamaya, S. Shimomura, Y. Fujii, S. Kishimoto, and H. Iwasaki, Solid State Commun. **76**, 443 (1990).

[15]A. Gibaud, H. You, S. M. Shapiro, and J. Y Gesland, Phys. Rev. B **44**, 2437 (1991).

[16]R. A. Cowley, G. Shirane, H. Yoshizawa, Y. Uemura, and R. J. Birgeneau, Z. Phys. B **75**, 303 (1989).

[17]J. P. Hill, T. R. Thurston, R. W. Erwin, M. J. Ramstad, and R. J. Birgeneau, Phys. Rev. Lett. **66**, 3281 (1991).

[18]J. P. Hill, Q. Feng, R. J. Birgeneau, and T. R. Thurston, Phys. Rev. Lett. **70**, 3655 (1993).

[19]J. P. Hill, Q. Feng, R. J. Birgeneau, and T. R. Thurston, Z. Phys. B **92**, 285 (1993).

[20]D. Gibbs, D. R. Harshman, E. D. Isaacs, D. B. McWhan, D. Mills, and C. Vettier, Phys. Rev. Lett. **61**, 1241 (1988).

[21]Doon Gibbs, G. Grubel, D. R. Harshman, E. D. Isaacs, D. B. McWhan, D. Mills, and C. Vettier, Phys. Rev. B **43**, 5663 (1991).

[22]J. P. Hannon, G. T. Trammell, M. Blume, and D. Gibbs, Phys. Rev. Lett. **61**, 1245 (1988).

[23]M. F. Collins, *Magnetic Critical Scattering* (Oxford University Press, New York, 1989).

[24]Yoseph Imry and Michael Wortis, Phys. Rev. B **19**, 3580 (1978).

[25]D. P. Osterman, K. Mohanty, and J. D. Axe, J. Phys. C **21**, 2635 (1988).

[26]T. C. Lubensky and M. H. Rubin, Phys. Rev. B **12**, 3885 (1975).

[27]A. Goldman, K. M. Mohanty, G. Shirane, T. R. Thurston, C. J. Peters, R. J. Birgeneau, R. L. Greene, and P. M. Horn, Phys. Rev. B **36**, 5609 (1987).

[28]T. R. Thurston, C. J. Peters, R. J. Birgeneau, and P. M. Horn, Phys. Rev. B **37**, 9559 (1988).

[29]W. C. Koehler, J. W. Cable, M. K. Wilkinson, and E. O. Wollan, Phys. Rev. **151**, 414 (1966).

[30]Doon Gibbs, D. E. Moncton, K. L. D'Amico, J. Bohr, and B. Grier, Phys. Rev. Lett. **55**, 234 (1985).

[31]J. Jensen and A. R. MacIntosh, *Rare Earth Magnetism* (Clarendon, Oxford, 1991).

[32]P. Bak and D. Mukamel, Phys. Rev. B **13**, 5086 (1976).

[33]H. Kawamura, Phys. Rev. B **38**, 4916 (1988).
[34]J. Eckert and G. Shirane, Solid State Commun. **19**, 911 (1976).
[35]G. H. F. Brits and P. de V. du Plessis, J. Phys. F **18**, 2659 (1988).
[36]B. D. Gaulin, M. Hagen, and H. R. Child, J. Phys. (Paris) Colloq. **49**, C8-327 (1988).
[37]K. D. Jayasuriya, S. J. Campbell, and A. M. Stewart, J. Phys. F **15**, 225 (1985).
[38]J. Wang, D. P. Belanger, and B. D. Gaulin, Phys. Rev. Lett. **66**, 3195 (1991).
[39]D. A. Tindall, M. O. Steinitz, and M. L. Plumer, J. Phys. F 7, L263 (1977).
[40]Z. Barak and M. B. Walker, Phys. Rev. B **25**, 1969 (1982).
[41]P. Azaria, B. Delamotte, and T. Jolicouer, Phys. Rev. Lett. **64**, 3175 (1990).
[42]Ames Laboratory sample information brochure.
[43]P. J. Schultz and K. G. Lynn, Rev. Mod. Phys. **60**, 701 (1988).
[44]M. Blume, J. Appl. Phys. **57**, 3615 (1985).
[45]W. Marshall and R. D. Lowde, Rep. Prog. Phys. **31**, 705 (1968).
[46]H. E. Stanley, *Introduction to Phase Transitions and Critical Phenomena* (Clarendon, Oxford, 1971).
[47]J. E. Lorenzo (private communication).
[48]Jin Luo, G. T. Trammell, and J. P. Hannon, Phys. Rev. Lett. **71**, 287 (1993).
[49]P. Carra and B. T. Thole, Rev. Mod. Phys. (to be published).
[50]M. Blume, in *Proceedings of the 2nd International Conference on Anomalous Scattering,* edited by K. Fischer, G. Materlich, and C. J. Sparks (Elsevier, Amsterdam, 1993).
[51]Helgesen *et al.* of Ref. 5 have found $\beta=0.41\pm0.04$ by x-ray-scattering studies on the same sample. This value agrees with the present value to within the errors. Helgesen *et al.* used a different range of temperatures and a smaller range of values for T_N when fitting order parameter data.
[52]T. Riste, E. J. Samuelsen, K. Otnes, and J. Feder, Solid State Commun. **9**, 1455 (1971).
[53]S. M. Shapiro, J. D. Axe, G. Shirane, and T. Riste, Phys. Rev. B **6**, 4332 (1972).
[54]A. D. Bruce and R. A. Cowley, Adv. Phys. **29**, 220 (1980).
[55]G. Shirane, R. A. Cowley, M. Matsuda, and S. M. Shapiro, Phys. Rev. B **48**, 15 595 (1993).
[56]J. D. Axe (private communication).
[57]Y. Imry and S. Ma, Phys. Rev. Lett. **35**, 1399 (1975).
[58]The walls of the long length scale domains in this system should be sharp because the correlation length ξ is smaller than the domain size l.
[59]M. Hagen, H. R. Child, J. A. Fernandez-Baca, and J. L. Zarestky, J. Phys. Condens. Matter **4**, 8879 (1992).

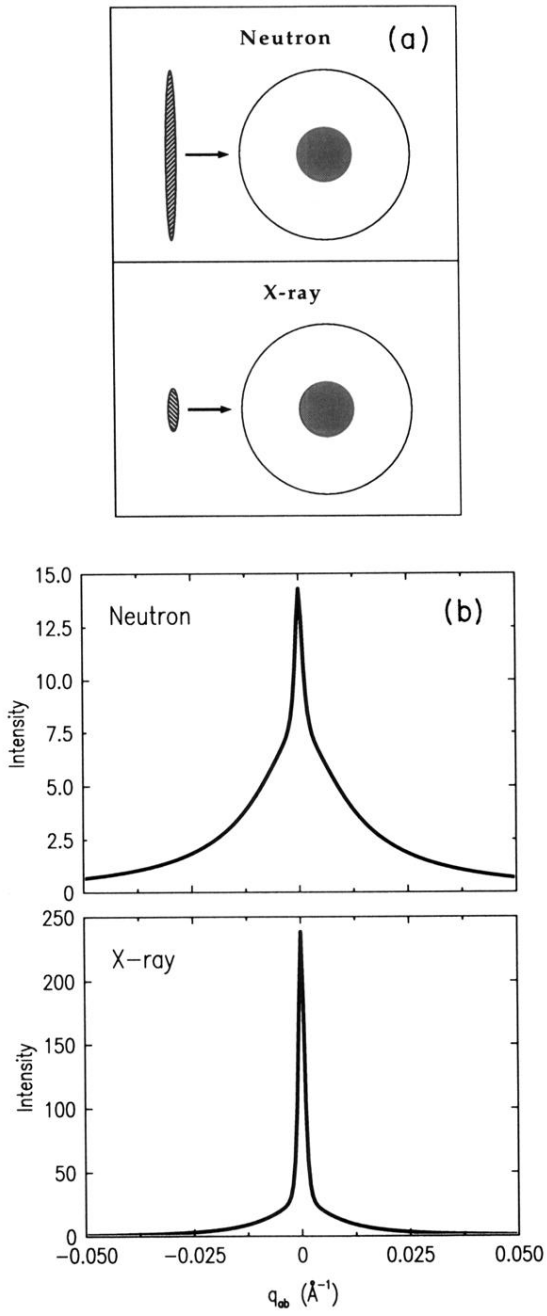

FIG. 12. (a) Pictorial representation of the x-ray and neutron resolution functions being scanned transversely through a two-component line shape. (b) Simulations of transverse scans where identical Lorentzian plus squared-Lorentzian line shapes have been convolved with the x-ray- and neutron-scattering resolution functions. The difference in visibility of the broad component here arises solely from resolution effects.